Optical Materials 169 (2026) 117646

Contents lists available at ScienceDirect

Optical Materials

journal homepage: www.elsevier.com/locate/optmat

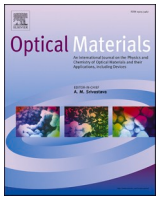

Research Article

Solid-state electro-active photonic crystals based on Tantalum-doped Titanium Dioxide multilayers☆

Cristina Mancarella [a,*], Liliana Moscardi [b], Giancarlo Terraneo [c,d], Alessio Lamperti [e], Marzia Iarossi [f], Francesco De Angelis [g], Francesco Scotognella [h,**], Andrea Li Bassi [a,d,***]

[a] Nanolab, Department of Energy, Politecnico di Milano, Via Lambruschini 8, 20156, Milano, Italy
[b] Department of Physics, Politecnico di Milano, Piazza Leonardo Da Vinci 32, 20133, Milano, Italy
[c] SupraBioNanoLab, Department of Chemistry, Materials and Chemical Engineering, Politecnico di Milano, Piazza Leonardo Da Vinci 32, 20133, Milano, Italy
[d] CNST Center for Nanoscience and Technology, Istituto Italiano di Tecnologia, Via Rubattino 81, 20134, Milano, Italy
[e] IMM Institute for Microelectronics and Microsystems, National Research Council CNR, Via C. Olivetti, 220864, Agrate Brianza, Italy
[f] Department of Biomedical Engineering, Technion–Israel Institute of Technology, 32000, Haifa, Israel
[g] Istituto Italiano di Tecnologia, Via Morego 30, 16163, Genova, Italy
[h] Department of Applied Science and Technology, Politecnico di Torino, Corso Duca degli Abruzzi 24, 10129, Torino, Italy

ARTICLE INFO

Keywords:
Electro-active photonic crystals
Nanostructured multilayers
Tunable photonic band gap
Transparent conductive oxides
Pulsed laser deposition
Multifunctional active-tunable devices

ABSTRACT

Photonic crystals can manipulate light by impeding transmission through photonic band gaps (PBGs), unlocking vivid structural colors and beating conventional spectrally-selective pigments. Nowadays, research is targeting at active and electrically-driven devices, moving beyond stacks of inert dielectrics. Plasmonic Transparent Conductive Oxides (TCOs) become appealing owned to their adjustable charge carrier density upon external stimuli (electrical biases), that enable electro-active control even in complex photonic architectures. Here, pioneer compact/porous one-dimensional PC multilayers, completely solid and entirely based on the novel and earth-abundant Tantalum-doped Titanium Dioxide TCO (Ta:TiO_2), have been developed with pulsed laser deposition through an original one-step method, by mastering the oxygen supply at deposition. Engineered doping and geometry enable tunable PBGs in the visible range. Electro-doping achieves PBG blue-shifts of 11–16 nm under low bias ($\leq$7 V) without liquid electrolytes. These findings unveil the potential of actively-tunable Ta:TiO_2 PCs to foster technological advancements in electro-optic switches, biosensors and anticounterfeit devices.

1. Introduction

The optical properties of photonic crystals (PCs) have become a core point of investigation in the optics and photonics community [1–5]. Indeed, PCs are structures characterized by periodic arrangement of two or more materials, each exhibiting distinct refractive index, with one-, two-, or three-dimensional pattern at a length scale comparable to the wavelength of light [1,6,7]. After suitably tailoring the geometry, the Bragg diffraction condition can be met generating a forbidden gap for the propagation of photons, i.e. the photonic band gap (PBG), at which most of the light is reflected backwards. This in turn activates bright and vivid structural reflection colors, arising only from geometrical architectures and not constrained by the spectrally-selective absorption properties of organic dyes or chemical pigments.

The most straightforward example of a one-dimensional (1D) PC is a layer-by-layer 1D stacking of different materials, whose easiness in fabrication provides the flexibility to incorporate polymers, glasses, semiconductors, or even biological materials. PCs of this kind can be found in nature and can be fabricated artificially by means of several methods, for instance sputtering [8], spin coating [9], and pulsed laser deposition (PLD) [10]. Specifically, PLD is known for its capability in growing a variety of materials with exceptional stoichiometric control, including metals and metal oxides, and eventually emerged as a promising method to produce high-quality PCs possessing high

☆ Given his role as Editor for this journal, Francesco Scotognella had no involvement in the peer review of articles for which he was an author and had no access to information regarding their peer-review. Full responsibility for the peer-review process for this article was delegated to another Editor.

* Corresponding author.
** Corresponding author.
*** Corresponding author. Nanolab, Department of Energy, Politecnico di Milano, Via Lambruschini 8, 20156, Milano, Italy.
E-mail addresses: cristina.mancarella@polimi.it (C. Mancarella), francesco.scotognella@polito.it (F. Scotognella), andrea.libassi@polimi.it (A.L. Bassi).

https://doi.org/10.1016/j.optmat.2025.117646
Received 23 May 2025; Received in revised form 25 September 2025; Accepted 22 October 2025
Available online 2 November 2025

reproducibility, yield and precision [11,12].

Nowadays, the rising concern towards multifunctionality and post-synthesis tunability of the photonic optical response of PCs, has stimulated the research to dig deeper into actively-modulated, electrically-driven nanosystems beyond inert stacks of dielectrics [3,13–15], whose main degree of freedom in controlling the optical outputs are the material choice and the PC geometry. The consequences on the application side are huge, enabling important technological advancements in displays, smart windows, optical cavities, solar cells and sensors. Several ways have been exploited to trigger the electric tunability of PCs, such as the reorientation of infiltrated liquid crystals, electrochemical processes, electrophoresis and field effect [13,15,16]. However, most methods rely on the employment of liquid electrolytes, which surely poses chemical and environmental issues, to be added to a faster degradation of the responsivity of the PC material by electrochemically-induced defects and detrimental structural hysteresis [17–19].

For all these reasons, all solid-state devices exhibiting field-effect tunability, i.e. exploiting injection/depletion of charges at biased semiconductor/insulator interfaces, are undoubtedly the most breakthrough direction of development to be pursued. To suit the quest, alternative plasmonic materials and especially the subclass of transparent conductive oxides (TCOs), are rightly called at play. TCOs are doped semiconductors that have previously caught the attention in the plasmonic, nanophotonic and optoelectronic sectors because of the high visible transparency and metal-like transport properties, along with a modifiable charge carrier density (spanning 10^{19} - 10^{21} cm^{-3}), significantly lower than that of metals (10^{22} cm^{-3}), thus leading towards plasmonic features extending up to the infrared region, not reachable by metal nanosystems that conventionally resonate in the visible [20].

The implementation of TCOs within multilayer PCs of the type doped semiconductor/insulator is very appealing but not much explored. Indeed, the key aspect is the innate carrier density tunability through external electrical stimuli, feature unbearable by classical metals, that permits the redistribution of carriers to modify the refractive index of the TCO, and hence the collective optical response of the PCs through the refractive index contrast [21–23]. Within the few existing examples, the role of the active layer is played by the TCO, and revealed successful in tuning the optical/plasmonic characteristics by exploiting photo-doping and electro-doping techniques [24–27]. For example, an active-tunable 1D PC have been realized with Indium-doped tin oxide (ITO) coupled with TiO_2 as dielectric element, revealing good performances in electrical responsivity (maximum PBG blue-shift of 23 nm upon 10 V) [16]. However, the scarcity of indium pushes towards the usage of earth-abundant and not-toxic TCO materials, such as Ta-doped TiO_2 (Ta:TiO_2), for which a fine control over the optical/electronic properties has been recently demonstrated through PLD fabrication [28–30].

In this work, we developed active-tunable transparent and conductive 1D multilayer PCs completely based on Ta-doped TiO_2, obtained in an original, one-step synthesis with PLD by alternating compact/conductive and porous/insulating TCO layers starting from the deposition of the same material. The refractive index contrast and the different optoelectronic characteristics between conducting and insulating units is solely granted by changing the background pressure of oxygen during the deposition, known to master morphology and stoichiometry (through oxygen vacancies) directly at the deposition stage [28,31,32]. The one-step synthesis approach is unique, as the realization of a high-quality actively-tunable 1D PCs completely based on the same TCO, up to the authors knowledge, has never been reported. PCs with different degree of doping (5 % and 10 % at. Of Ta, i.e. Ta(5 %)TiO_2 and Ta(10 %):TiO_2) and variable geometries have been realized to create PCs with PBG localized in the visible range, experimentally showing active modulation of their PCs characteristics upon the application of an external electrical bias. Indeed, the PBG blue-shifts up to 11–16 nm with relatively low voltages (maximum at 7 V). The investigation has been enriched with detailed material characterization of morphological and structural properties of the single components, as well as the overall optical properties of the PC multilayers with or without bias applied. The discussion of the physical mechanisms at play, attributed to electro-doping and accumulation/depletion processes, has been supported by theoretical simulations based on transfer matrix method.

2. Experimental Section

***Material synthesis*:** the synthesis of 1D PC multilayers was performed with Pulsed Laser Deposition (PLD) in a vacuum chamber equipped with a primary and turbomolecular pumping system, gas inlets and mass flow controllers to monitor the partial pressure of gaseous species during the deposition process. All multilayers are completely based on Ta:TiO_2 and were fabricated at room temperature by depositing sequentially compact and nano-porous layers via PLD in a one-step method without breaking the vacuum. This was done by setting the background oxygen atmosphere at 1 Pa O_2 in case of compact layers, or at 6 Pa O_2 for the porous layers. These conditions of deposition pressures have been selected first in order to maximize the optical contrast (difference between the refractive index of the components, Δn), as it is known from photonic crystal theory to intensify Bragg diffraction and the Photonic Band Gap (PBG) bandwidth [10], but also to simultaneously obtain both a conductive, actively tunable layer (at 1 Pa) and a dielectric one (at 6 Pa) within the same deposition process. The optical contrast is further intensified by the variation in morphology from compact to porous structures.

The laser source for the material synthesis is a ns-pulsed Nd:YAG laser (2nd harmonic, $\lambda = 532$ nm green, repetition rate 10 Hz and pulse duration 5–7 ns). The pulsed laser beam is focused on the target material with an angle of 45° with respect to the normal direction of the target surface, subjected to roto-translation to ensure a uniform ablation. The investigated photonic crystals are based on Ta:TiO_2 with 5 % and 10 % at. Of Ta (also referred as TCO Ta 5 % and TCO Ta 10 % or Ta(5 %):TiO_2 and Ta(10 %): TiO_2), fabricated by ablating Ta_2O_5: TiO_2 targets (99.99 % purity) with molar ratio 0.025:0.975 and 0.05:0.95 respectively, all provided by "Testbourne Ltd". The laser fluence on the targets was set to 2.27 J cm^{-2} for Ta(5 %): TiO_2, and 2.73 J cm^{-2} for Ta(10 %):TiO_2. The fluence was varied by keeping the pulse energy fixed at 150 mJ, while modifying the spot area onto the target from 6.6 mm^2 to 5.5 mm^2. Ta:TiO_2 films with 10 % at. Of Ta required a higher fluence in order to avoid delamination and maximize compactness and crystallinity. As-deposited Ta:TiO_2-based PCs are obtained at room temperature and are amorphous, thus annealing treatments are necessary to achieve crystallization of the compact layers in single phase polycrystalline TiO_2 anatase. Thus, post-deposition annealing in a reducing atmosphere (e.g., vacuum) is required to maintain the oxygen-substoichiometry contributing to conduction in compact TiO_2-based TCOs [42] (compact layers), performed in a furnace designed for thermal treatments in vacuum at 550 °C (base pressure 5×10^{-5} Pa), 1 h dwell at 10 °C/min ramp.

All systems were deposited over commercial indium tin oxide (ITO) substrates (ITO-coated glass, with sheet resistance 10 Ω sq^{-1}, purchased from XOP Glass), mounted on a rotating sample holder with fixed target-to-substrate distance (50 mm). Substrates were cleaned in ultrasonic bath with isopropanol for 20 min prior to deposition.

In this work we investigated two multilayer geometries differing in the thickness ratio (TR), obtained by dividing the thicknesses (measured at SEM) of the compact (synthetized at 1 Pa O_2) and the porous layers (at 6 Pa O_2) and referred in the text as low TR (1.01) or high TR (1.3). The single layer thicknesses have been selected to maximize visible light reflection with these combinations of materials and porosity, hence possessing a distinctive PBG within 500–600 nm, with the aid of home-made Matlab codes based on Transfer Matrix Methods [33–35]. The geometries selected for Ta(5 %):TiO_2 and Ta(10 %):TiO_2 multilayers are summarized in Table 1. A brief description of the TMM theory, the code employed and the parameters changed to perform the simulations have been inserted in a brief comment in the Supporting Information.

Table 1
Optimized geometry (thicknesses of compact and porous repeating units) for Ta (5 %): TiO_2 and Ta(10 %):TiO_2 multilayer PCs. Two set of samples have been identified, according to the thickness ratio (TR) between compact and porous layers: low TR (1.01) and high TR (1.3). The thicknesses reported are the mean of real thickness values of compact and porous constituents, as extracted from SEM images.

	Low TR		High TR	
Ta content (at. %)	***5 %***	***10 %***	***5 %***	***10 %***
Compact unit thickness (nm)	63	74	85	89
Porous unit thickness (nm)	62	73	65	65
Actual compact/porous thickness ratio	1.016	1.013	1.30	1.37
Average compact/porous thickness ratio	**1.01**		**1.3**	

Finally, electrical contacts were integrated on PC multilayers to create a device for electro-optical measurements. The ITO substrate is the bottom electrode while the top electrode was obtained by thermally evaporating 50 nm of Ag (Edwards E360 thermal evaporator) on half part of the multilayer surface. The electrical circuit is closed by using copper wires bonded to the top and bottom electrodes with silver paste.

Material characterization: the morphology of Ta:TiO_2-based PCs was characterized by field emission Scanning Electron Microscopy (FEG-SEM, Zeiss SUPRA 40), in cross-section for ad-hoc samples deposited on silicon substrates.

X-ray diffraction (XRD) patterns on single Ta:TiO_2 layers deposited at 1 Pa O_2 (compact) and 6 Pa O_2 (porous), were collected using a Bruker D8 Advance X-ray diffractometer at 293 K (Cu K-α radiation, 1.5406 Å). The measurements were carried out in a Bragg–Brentano geometry (θ-2θ) with a step-scan technique and a 2θ range of 10–90°. Data were acquired by using a Lynx Eye detector in continuous scanning mode with a step size of 0.038 and a time step of 0.15 s. The grazing incidence (GI) measurements were carried out with an incidence angle of 0.95°.

The XRD measurements in Bragg–Brentano and grazing incidence geometry were carried out under the same measured range and measurement conditions (scanning mode, step size, and time per step).

For X-ray reflectivity (XRR) measurements on single compact and porous Ta:TiO_2 references, an HRD3000 diffractometer (Italstructure) operating with monochromated x-ray tube (Cu K-α at $\lambda = 0.1541$ nm) was used, conditioned in parallel configuration by a parabolic mirror and defined by 0.18 × 4 mm source slits and equipped with a point-type NaCl(Tl) scintillator detector, with 0.2 mm accetpance slits on the detector arm. XRR scans were collected in a specular ω-2θ geometry, in the range ω = 0–4°, in steps ω = 0.01°.

Electrical properties and Hall effect measurements of single Ta:TiO_2 layers deposited at 1 and 6 Pa O_2 were carried out in the four-point probe configuration with a Keithley K2400 Source/Measure Unit as a current generator (from 100 nA to 10 mA), an Agilent 34970A voltage meter, and a 0.57 T Ecopia permanent magnet.

The set-up of Spectroscopic Ellipsometry is based on a J.A. Woollam V-VASE ellipsometer. Specifically, single Ta:TiO_2 layers deposited at 1 and 6 Pa O_2 on glass substrates and with an expected thickness of 200 nm were measured from 300 nm to 1700 nm for angles of incidence equal to 45° and 60° to determine their optical constants. The experimental data were fitted by using the optical constants of Palik model for the glass substrate, and with Tauc-Lorentz oscillator and Drude model to simultaneously account for the interband absorption at the energy gap in the ultraviolet, and NIR free-carrier absorption tail. The roughness of the surface was taken into account by adding a top thin layer of few nanometers modelled by a Bruggemann effective-medium layer made of 50 % by Ta:TiO_2 and 50 % by voids.

For electro-optical measurements in transmission (range 350–1050 nm, at normal incidence), we used a fiber-coupled spectrometer (Avantes, AvaSpec-HS2048XL-EVO), with the external bias applied with an Agilent 6614C source-meter. The voltage has been varied between 0 V and 7 V. Moreover, the same measurement has been performed forward (increasing the voltage) and backward (decreasing the voltage) to ascertain the reversibility of the process. Seldomly, the applied bias causes the breaking of the substrate, hence the backward measurements were not possible, and limiting the maximum voltage to 5 V. These are likely due to stochastic effects such as Joule heating of the amorphous glass substrate, rather than an intrinsic limitation of the material or device design. To appreciate the PBG shift, the time difference between evaluation of the spectra in unbiased and biased situation is 1 min.

Optical reflectance spectra (range 300–1100 nm) were evaluated on samples deposited on ITO substrate with a UV–vis–NIR PerkinElmer Lambda 1050 spectrophotometer equipped with a 150 mm diameter integrating sphere. This setup enables the measurement of total reflectance, meaning that light reflected by the film is collected at all angles. All the acquired spectra were normalized with respect to the ITO substrate contribution.

3. Results

3.1. Morphology, structure and electrical properties of Ta(5 %):TiO_2 compact and porous single layers

Before analyzing the overall electro-optical response of Ta:TiO_2-based PCs multilayers, morphological, electrical, and structural properties of the compact and porous constituents after thermal treatments have been investigated in detail from a material science perspective. SEM images of Ta(5 %):TiO_2 (also referred as TCO Ta 5 %) reference samples of 200 nm thickness deposited at 1 Pa and 6 Pa of O_2 background pressure are reported in Fig. 1a and b. The former exhibits a compact morphology. When rising the deposition pressure from 1 to 6 Pa O_2, compactness is lost and a transition to a nanoporous architecture occurs, characterized by a hierarchical tree-like morphology and cluster-assembled nanoparticles of few nm typical of PLD-grown materials [36,37].

The crystalline structure of single layer references has been investigated via X-Ray diffraction, whose technical details are described in the Experimental Section. Fig. 2 shows XRD diffractograms of compact (synthetized at 1 Pa O_2) and porous (at 6 Pa O_2) layers with 5 % at. Of Ta, with thickness of 200 nm on glass substrates. The compact layer measured in Bragg-Brentano (*θ-2θ*) configuration (black curve) presents a defined structure, with the most intense peaks associated to the (101) (004) and (200) planes of polycrystalline anatase TiO_2 phase [40], in line with previous literature [28,31]. The predominant orientation occurs along the (101) surface, the one possessing the lowest surface energy [41]. The mean crystallite size calculated with the Scherrer equation from the most intense (101) peak, is 44.2 nm. For the porous counterpart instead (blue curve), the film is amorphous as no diffraction peak is detected, thus suggesting that anatase crystallization is hindered by the high degree of porosity and defectivity introduced at higher deposition pressures [28,42]. XRD in grazing incidence angle has been performed on the porous reference in order to enhance the surface sensitivity of the technique and intensify possible weak signals. Diffraction peaks related to TiO_2 anatase are still absent, as in *θ-2θ* configuration, confirming that the porous system is mainly amorphous; although weak and broad peaks can be referred to (111), (210), (411) and (621) surfaces of the allotrope rutile phase of TiO_2, hence indicating that a small amount of rutile nanocrystallites grew in a prevailing amorphous matrix. The presence of rutile has been previously reported in TiO_2 nanostructures grown by PLD at higher O_2 background pressure [43,44], where in-plume nucleation of rutile clusters is expected directly during synthesis, as the anatase-to-rutile transition occurs above the typical annealing temperature reached in this work [45]. Indeed, as-deposited rutile nanocrystallites serve subsequently as crystallization seeds during post-deposition thermal treatments.

X-Ray reflectivity measurements have been performed on TCO Ta 5 % references, with the aim to underline differences between compact

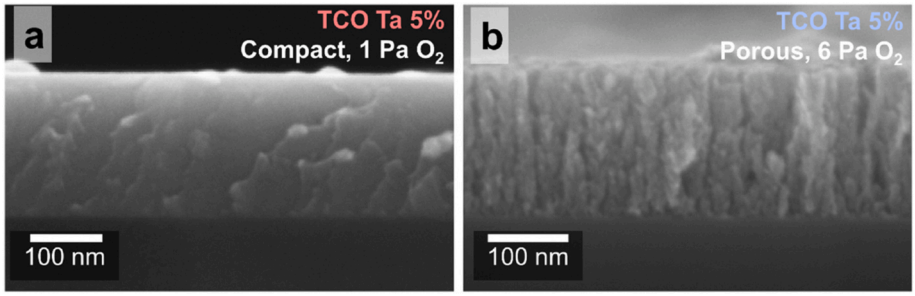

Fig. 1. SEM cross-section images of compact (a) and porous (b) reference films of Ta(5 %):TiO_2, obtained respectively at 1 Pa O_2 and 6 Pa O_2, with thickness of 200 nm on Si(100).

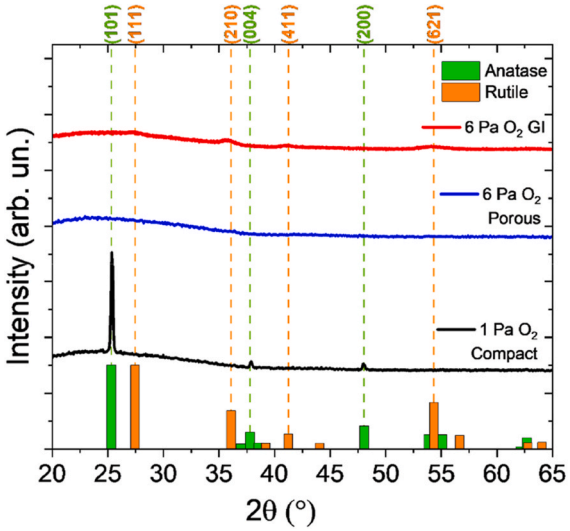

Fig. 2. XRD diffractograms of single layer references for compact (synthetized at 1 Pa O_2) and porous (at 6 Pa O_2) Ta(5 %):TiO_2 films, followed by thermal treatment in vacuum, with thickness of 200 nm on glass. The measurements have been performed in Bragg-Brentano (θ-2θ, black and blue lines) or grazing incidence (GI, red lines) configuration. Characteristic peaks of anatase (green) and rutile (red) TiO_2 bulk phases taken from Minkrist database [38,39] are shown for comparison.

and porous units in terms of surface morphology, i.e. roughness, thickness and density with high degree of precision [46]. The compact layer exhibits a roughness of around 1.1 nm, while for the porous counterpart is roughly 4.4 nm. The electron density of thin films can be obtained from the determination of the critical angle at which incident X-rays are totally reflected, and then converted into mass density. The compact layer possesses a mass density of 4.83 g cm^{-3}, slightly higher than bulk density tabulated for TiO_2 (≈3.7–3.9 g cm^{-3}) [47,48], due to the aliovalent substitution of Ti with Ta owning a higher atomic number. The porous layer instead is characterized by a mass density of 2.56 g cm^{-3}, confirming that the increase in deposition O_2 pressure from 1 to 6 Pa is associated to a reduction of mass density due to the higher amount of nano-voids already detected in SEM images [49]. It is possible to estimate more explicitly the porosity, by computing the ratio between the mass density of the compact and the porous layer achieved form XRR (2.56 g cm^{-3} and 4.83 g cm^{-3}, respectively). Therefore, it can be inferred that the mass density in the porous film has been reduced of 47 % with respect to the compact, void-free counterpart. Therefore, 47 % can be taken as reasonable indication of the void porosity percentage.

Electrical measurements performed on the compact Ta(5 %):TiO_2 reference give a resistivity of 7.41 × 10^{-4} Ω cm, mobility equal to 6.9 $cm^2 V^{-1} s^{-1}$ and electronic carrier density N of 1.22 × 10^{21} cm^{-3}, further confirming that the synthesis at 1 Pa O_2 accomplishes the metal-like behavior, besides the highest conducting properties for n-type Ta-doped TiO_2 [28,31]. At 10 % at. Of Ta doping (Ta(10 %):TiO_2, also referred as TCO Ta 10 %), resistivity is expected to be similar as for 5 % at. Of Ta, although the mobility reduced (4 $cm^2 V^{-1} s^{-1}$) and the electronic carrier density increased (1.65 × 10^{21} cm^{-3}) [31]. The porous component obtained at 6 Pa O_2 is insulating as too resistive and not electrically measurable with our experimental setup, as foreseen by the combination of an amorphous nature and an open-void network of porosity and high oxygen environment during PLD. Mazzolini et al. [28] already reported for similar Ta:TiO_2 films a strong dependence between the electrical properties and the oxygen background pressure kept during synthesis, showing that above 2.25 Pa of O_2, resistivity increases of one order of magnitude with respect to films achieved at 1 Pa O_2, while carrier density and mobility degrade consistently (to ≈ 10^{20} cm^{-3} and 6 $cm^2 V^{-1} s^{-1}$ respectively). The drop in electrical conduction is a consequence of the strong confinement of the motion of carriers, due to defects, nano-voids and surface states introduced upon nanostructuring, acting as trapping sites for free electrons [43,50]. Ta atoms are still present in the material but the high level of defectivity leads to ineffective doping. In addition, the loss of substoichiometry is detrimental for electrical performances because oxygen vacancies are known to contribute consistently to electronic conduction in vacuum-annealed TiO_2-based semiconductors as double negative charged donor states [28,31,32,51–53].

The mechanism behind this easy-achievable and versatile modulation of porosity and morphology (and crystallinity) of metal oxides is inherent in the PLD technology, as fully described elsewhere [10,36], and here efficiently exploited in an original way to develop an easy-to-handle and one-step deposition procedure for porous/compact Ta:TiO_2 PC multilayers. The method followed in this work is schematized in Fig. 3. The originality and most important advantage rely on the utilization of the same target material, i.e. Ta:TiO_2 with 5 % or 10 % at. Of Ta doping, from which multilayers alternating compact and porous constituents are achieved straightforward, without breaking the vacuum, by varying the background deposition atmosphere of oxygen. The number of layers have been fixed to 10, recognized as the best compromise between fabrication efficiency and adequate photonic performance, and to facilitate a broader comparison with similar multilayers found in literature [17,19,54]. Comparison between transmission of PCs using 10 or 20 repeating layers simulated by Transfer Matrix Method (TMM) [33,35] has been reported in Fig. S1. Different geometries and doping levels (5 % and 10 % at. Of Ta) have been explored, as explained in the Experimental Section. In particular, PCs have been discussed according to the thickness ratio (TR), obtained by dividing the thicknesses of the compact and porous units, as retrieved from SEM images (more details in the Experimental Section, Table 1).

This parameter indicates the relative content in the PC of compact and porous counterparts, that will be essential in determining the optical response. In this work, TR is kept higher than one (the compact layer thicker than the porous counterpart in both low and high TR configuration), because it is the condition able to maximize optical PC quality,

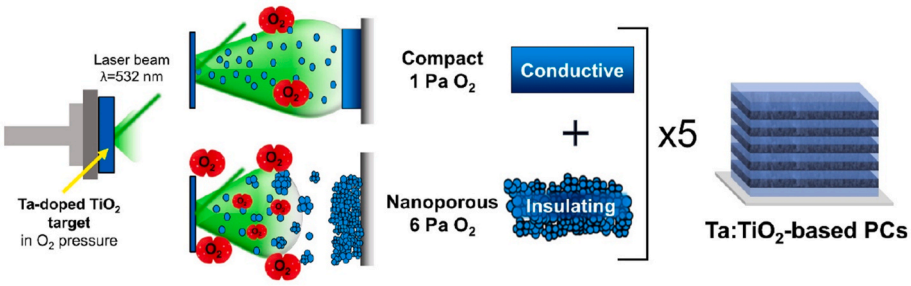

Fig. 3. Schematic representation of the synthesis procedure of Ta:TiO_2-based PCs multilayers by PLD.

as predicted by TMM simulations (see Experimental Section). SEM cross-section images of the resulting PCs with high TR (1.3) after thermal treatment are shown in Fig. 4a and b, with different doping degree. The multilayers show good homogeneity; the porous counterpart is squeezed between the compact layers, with highly continuous and interconnected interfaces (magnification in Fig. 4c). In this section, structural and electronic properties of single layers have been proved to vary widely, thus expecting a high refractive index contrast towards PCs possessing high optical quality. Moreover, being the compact layer conductive and with tunable carrier density through doping, active electrically-induced modulation of photonic features are possible, thus deeply investigated and discussed in the following sections.

3.2. Static optical properties of compact/porous Ta:TiO_2-based PCs

Prior to investigate the static optical characteristics of multilayers, spectroscopic ellipsometry has been performed on single compact and porous films of TCO Ta 5 % (Fig. 1) to acquire the real (n) and imaginary (k) parts of the complex refractive index (Fig. S2). Average n extracted from experimental data in the range 450–750 nm (2.75–1.65 eV) for compact and porous films are respectively 2.35 and 1.7, while the k component associated to absorption losses is almost zero in both cases. The refractive index contrast Δn is 0.65, higher than WO_3-based PCs [19] and in line with other oxide-based dense/porous PCs showing high reflection efficiencies [10,17,55–57]. This proves that our synthesis approach allows a noticeable difference in the microstructure of the alternating layers resulting in a large index contrast and an efficient and simultaneous modulation of mass density and carrier concentration of the same TCO material, ensuring a good optical contrast for the Bragg diffraction condition to be fulfilled at visible wavelengths. In addition, the role of the compact/porous interface, along with the carrier density of the compact layer, is foreseen to be essential in maximizing the electro-optic modulation, as it will be clarified later in the text.

Transmittance measurements in the UV-VIS-NIR range on TCO multilayers with 5 % and 10 % at. Of Ta doping have been performed in order to assess the optical quality of the PCs and characterize the photonic band gap at rest in 0-bias condition. Fig. 5 shows the transmittance of PCs with low and high TR (1.01 and 1.3 respectively) with different doping content (5 % and 10 % at. Ta). All spectra present a transmittance drop below 400 nm due to the optical band gap absorption in the UV of anatase TiO_2-related materials [58]. All the geometries show a transmittance dip in the visible, within 450–750 nm, associated to the PBG of the crystals, reflecting the green (Ta 5 %) and the red (Ta 10 %). The PBG wavelength λ_{PBG} and transmittance minimum T_{PBG} at the PBG are important parameters to be discussed further in the work, thus clearly indicated in Fig. 5 (first panel). Except for the abrupt loss at the photonic stop band, transmittance can reach 60–65 % in the region 400–500 nm and 750–900 nm, thus showing high transparency despite the consistent thickness (>700 nm), comparable to single films of 200 nm of Ta:TiO_2 (with mean transmittance within 60–80 %) [31]. This demonstrates the good optical quality characterizing these PCs with only 5 repeating bilayers composed of the same Ta:TiO_2 material, because of the high index contrast achieved directly at synthesis. Indeed, the geometries selected satisfy the general rule $d_b \approx \lambda_{PBG}\,(4n)^{-1}$ correlating the thickness of the bilayer d_b (120–140 nm) to the desired wavelength for maximum PBG reflection λ_{PBG} (500–600 nm) [1]. In the NIR region of the spectra, i.e. above 800 nm, the transmittance of TCO-based PCs starts reducing when the Ta doping is higher (10 % at.), due to the blue-shift of the free carrier absorption tail, i.e. higher plasma frequency [59,60], predicted for Ta:TiO_2 films in the mid-IR around 4–6 μm [31].

Fig. 6 shows λ_{PBG} (Fig. 6a) and T_{PBG} (Fig. 6b) as a function of the thickness ratio TR, evaluated from transmittance curves of multilayers in Fig. 5. The lowest is T_{PBG}, the higher is the efficiency of the PC stop band. In case of TCO Ta 5 % PCs the increase in TR, i.e. higher thickness of compact layer at the expense of the porous part, leads to a red-shift of λ_{PBG} in Fig. 6a from 570 nm (low TR) to 616 nm (high TR) and a slight increase in T_{PBG}, from 12 % to 16 % (Fig. 6b). The same trend can be qualitatively reproduced with TMM formalism (Fig. S3), but a perfect matching of the curves is hard to achieve due to optical losses and unwanted surface scattering deviating light at compact/porous discontinuities [19,61,62]. PCs based on higher Ta doping (10 % at.) follow the same trend in TR, although λ_{PBG} is red-shifted compared to Ta 5 % PCs (594 nm at low TR, 622 nm at high TR), with higher T_{PBG} (33 % at low

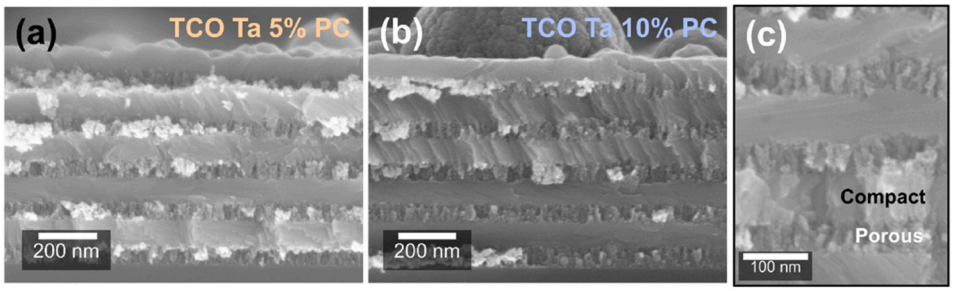

Fig. 4. SEM cross-section images of porous/compact PCs (obtained at 6 Pa/1 Pa O_2, followed by annealing in vacuum) with thickness ratio (TR) compact/porous equal to 1.3, based on TCO Ta 5 % (a) and TCO 10 % (b). (c) Magnification of porous/compact interface in TCO Ta 5 % PCs multilayer in (a), annealed in vacuum atmosphere at 550 °C.

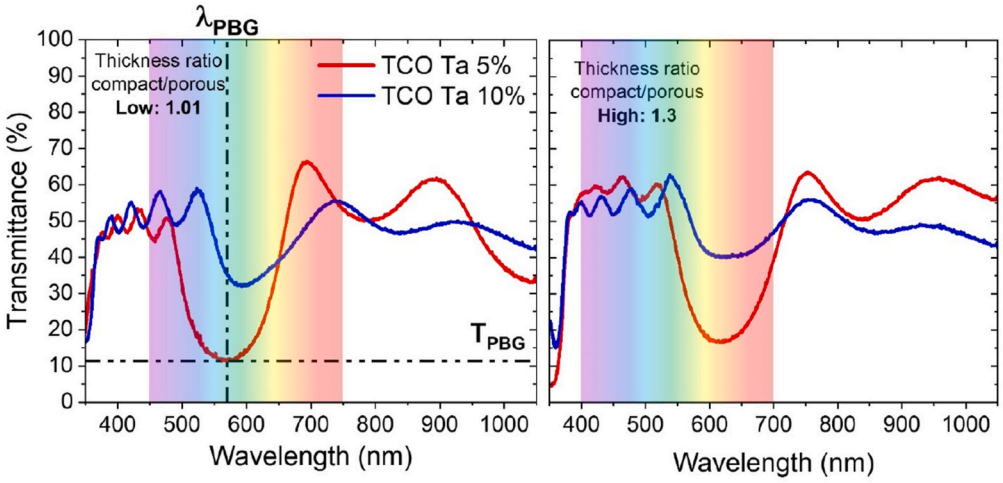

Fig. 5. Transmittance spectra at normal incidence on ITO substrate, without bias applied (0 V), for low 1.01 and high 1.3 thickness ratio (TR) PCs, based on TCO Ta: TiO_2 with 5 % and 10 % at. Of Ta content. In transmission spectrum of low TR (1.01), example of the determination of λ_{PBG} and T_{PBG} values on a real PC spectrum (TCO Ta 5 %) are shown.

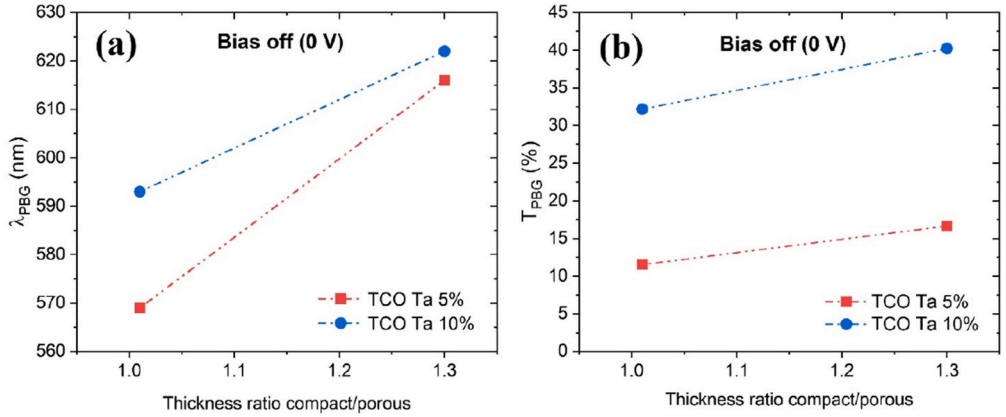

Fig. 6. PBG parameters λ_{PBG} (a) and T_{PBG} (b) as a function of the thickness ratio TR (between compact and porous layer) reported in Table 1, of PCs made of TCO Ta: TiO_2 with 5 % and 10 % at. Of Ta, without bias applied (0 V).

TR, 41 % at high TR), i.e. reduced reflection capability at the PBG. These differences can be ascribed to the variation in effective refractive index n_{eff} (weighted sum of n of the single constituents) and Δn, when varying the Ta doping, as regulated by the modified Bragg-Snell law [13,15,24,61,63–65].

Moreover, all the PBG characteristics discussed in transmission are consistent also in reflectance mode (Fig. S4). Interestingly, as a final remark, it should be underlined that the PBG characteristics, thus the PC operability, can be enlarged from the VIS to the infrared, appealing for thermal regulation [66,67], for instance by increasing the thicknesses of the repeating layers directly during the PLD synthesis, as simulated by TMM and reported in Fig. S5.

3.3. Electro-optical measurements

Ta:TiO_2-based PCs were tested for electro-optical modulation by applying an external electrical bias on the nanocomposite devices, according to the setup shown in Fig. S6, and then measuring the transmittance under applied potential.

To help with the interpretation of results, a brief recall to the basic electro-induced modifications of the refractive index of materials has been reported in the Supplementary Information. Electro-responsivity of the PBG stopband is expected in Ta:TiO_2-based PCs because the charge carrier density, and so n and Δn, varies in TCOs upon the application of an external electrical stimulus [68–71]. Indeed, the refractive index of a TCO material can be linked to the complex dielectric function ε, and hence the plasma frequency ω_p, through the Drude model, by following the state-of-art relations reported in the Supporting Information [72–74].

Optical and plasmonic properties of Ta-doped TiO_2 can be well described under the free-electron assumption of the Drude model, as long as the optical phenomena of interest are far from UV inter-band transitions owned by TiO_2 semiconductors. Moreover, TCOs with N approaching 10^{21} cm^{-3}, as fulfilled with both Ta 5 % and 10 % at. Ta: TiO_2, produce significant refractive index changes at visible frequencies triggered by external voltages [21,68,70]. Specifically, in our systems only the compact units are expected to be “bias-active”, being degenerate n-type semiconductors, crystalline and conductive, although the amorphous and insulating nature of the porous layer should prevent bias-induced transport of free carriers.

Transmittance curves before (dark gray line) and after (colored lines) bias application on PCs with Ta 5 % at. and 10 % at. with different TR values are shown in Fig. 7a and b. When the voltage is switched on up to 5–7 V (the maximum value reachable is limited by the mechanical failure of the substrate, see Experimental Section), the multilayers experience an overall reduction of transmittance, especially at λ_{PBG} (T_{PBG}), and a blue-shift of the PBG band, for all TR values. Concerning transmittance, T_{PBG} reduces within 2–4 % points in TCO Ta 5 % PCs,

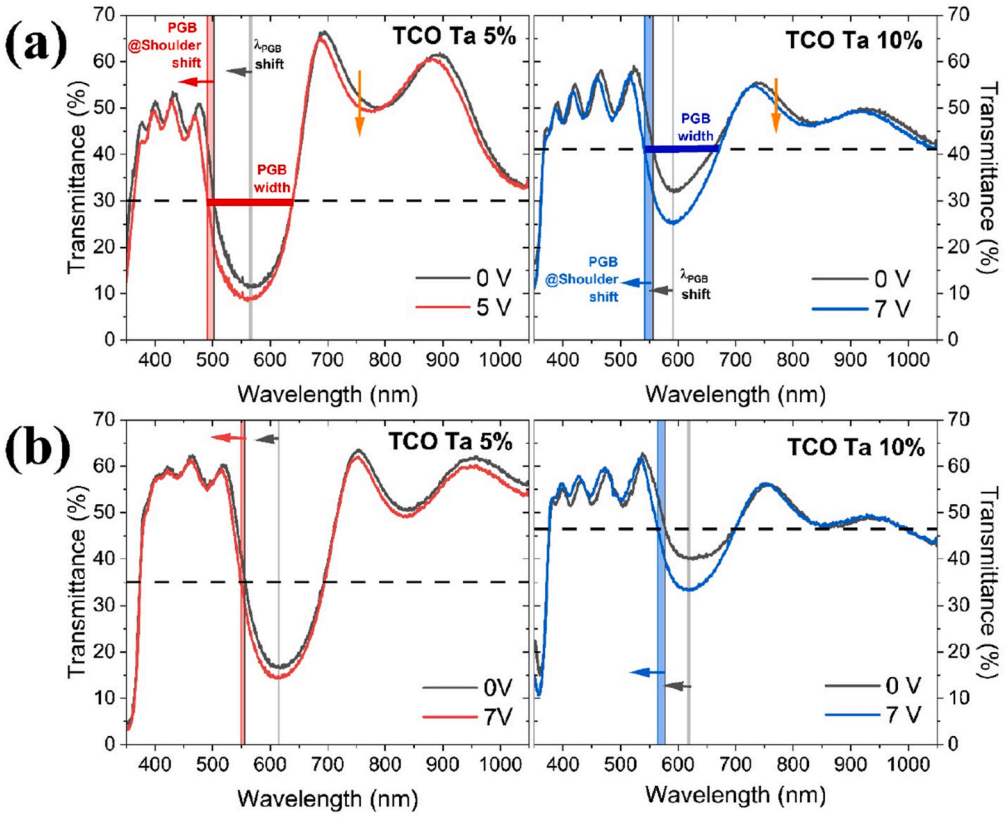

Fig. 7. Transmission spectra taken at normal incidence, with and without applied voltage, of Ta 5 % and 10 % PCs compact/porous (1 Pa/6 Pa O_2) for low (a) and high (b) TR. In (a) the electro-optic parameters discussed in the text are clearly indicated (PBG modifications evaluated at shoulder, λ_{PBG} shift and PBG width).

while the tunability is wider when increasing the Ta doping in TCO Ta 10 % PCs, where T_{PBG} diminishes of 4–10 % indicating an important role played by the static carrier density N. However, the λ_{PBG} only slightly modifies with the applied voltage in all the multilayers considered, with shifts of 5 nm or less. Indeed, to better appreciate the entity of electrical modulation upon bias, instead of considering λ_{PBG}, we will discuss from now on the wavelength shift occurring at the PBG shoulder, referred as PBG shift, i.e. the shift at the low-wavelength value taken approximately at half of the PBG transmittance dip (dashed horizontal lines in the spectra of Fig. 7), compared to the unbiased curve. In addition, also the variation of the PBG width, estimated at half of the transmittance dip, will be analyzed. These parameters are evidenced in Fig. 7a.

The extent of the PBG modifications turns out to be dependent from the Ta doping content and the geometrical characteristics (thickness ratio TR) of the multilayers, as analyzed in the graphs in Fig. 8 with the PBG shift and PBG width parameters. The precise numerical values for reference have been summarized in the table in Fig. S7, in the Supporting Information. Multilayers with lower TR (1.01) exhibit the maximum PBG blue-shift, reaching 11 nm at 5 V and 16 nm at 7 V for PCs with 5 % and 10 % Ta content, respectively. When increasing the thickness ratio (at 1.3, Fig. 8a), the shift reduces to 7 nm and 13 nm in case of 5 % and 10 % of Ta doping in the TCO PCs, respectively. Indeed, the optimal geometry (low TR) corresponds to a bilayer thickness of 63 nm (74 nm) for the compact part and 62 nm (73 nm) for the porous one, for TCO-based PCs with 5 % (10 %) at. Of Tantalum. At higher thickness ratio, the thickness of the compact layer increases with respect to the

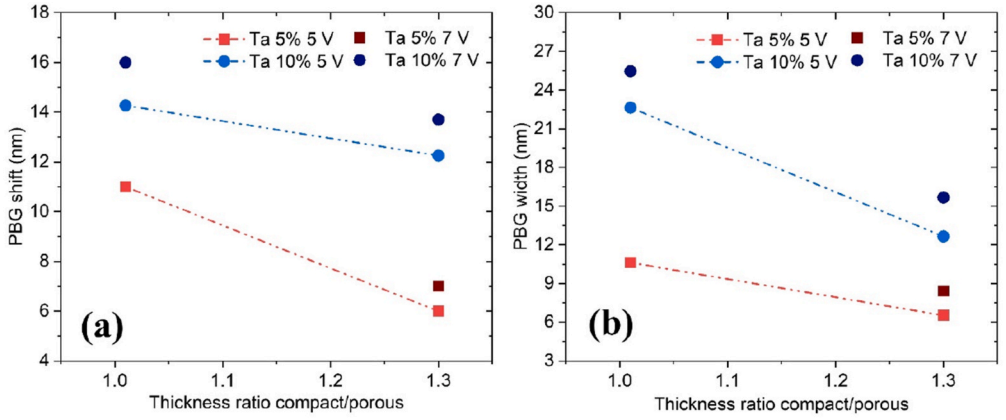

Fig. 8. (a) PBG shift taken at the PBG shoulder for PCs based on TCO 5 % and 10 % Ta, as a function of the thickness ratio compact/porous layers. (b) PBG width variation taken at the PBG shoulder for the same PCs in (a) as a function of the thickness ratio.

porous one (85/65 nm and 89/65 nm for 5 % and 10 % Ta). Noticeably, the PBG optical modulation is wider when increasing the Ta doping inside TCO-based PCs, as already noticed in Fig. 8, further underlying the important role played by the initial static value of the free carrier density. Fig. 8b shows that the trend in PBG shift with TR is retrieved in the PBG width, with a change in the width of PCs from 7 nm up to 26 nm. In addition, transmittance curves in Fig. 7 in initial 0-bias situation, have been compared with curves at 0-bias collected after voltage application, going backward ("0 V back") in Fig. S8 showing a good reversibility of the optical process in some minutes.

4. Discussion

As stated at the beginning of the previous section, the tunability in PBG characteristics is linked to the bias-induced variation of the refractive index achievable in a TCO layer. A blue-shift of the photonic stopband (λ_{PBG}) is foreseen under bias, as predicted by the modified Bragg Snell law previously cited, since λ_{PBG} is directly proportional to the refractive index of the constituent layers, that is expected to decrease in the compact TCO layer as a consequence of the active flowing and redistributions of free carriers at compact/porous interfaces (i.e. increase in the plasma frequency or formation of accumulated/depleted regions within the PC boundaries). However, the mechanism under study is complex and still debated, and more reasonably is the outcome of several bias-activated events appearing in TCO semiconductors. An attempt to explain these concepts is provided in the following paragraphs. To favor the comprehension, the main modulation mechanisms at play have been schematized in Fig. 9.

As a first possibility, the PBG blue-shift and transmittance reduction could be the result of the increase of ω_p in the compact/conducting TCO unit (Fig. 9a) as already noticed (i.e. a blue-shift of the onset of free carrier resonance), along with intensified light absorption (also known as Franz-Keldysh effect) [22,72,75,76], mediated by carriers injected under bias (electro-doping processes) [16,77]. This behavior can be foreseen also in our systems by simulating with TMM the transmittance response of PCs (Fig. S9) with rising carrier density, i.e. lower refractive index n, in the compact/conducting TCO layers (obeying to the Drude model) and a fixed n in the insulating one (as retrieved from ellipsometry on single layers, Fig. S2).

Electro-doping phenomena occurs by injecting carriers among layers through defects, i.e. at compact/porous interfaces, supplied by the external circuit. Oxygen vacancies present in sub-stoichiometric TiO_2-based semiconductors could mediate as injection points [78]. Indeed, oxygen vacancies in the proximity of dopants can develop systematic conductive filaments under applied bias, as demonstrated in ZnO or Ta_2O_5-based resistive switchers [78–81].

In this perspective, an additional effect could contribute to the modulation of PBG features, even if its direct investigation in the nanosystems here investigated is quite challenging. It is known that the application of an external voltage to a layered structure based on TCOs (e.g. ITO) repeated with insulators exhibits accumulation/depletion regions of free carriers at interfaces, with associated bias-induced decrease/increase of the local relative permittivity ε [74,82–85]. The impact of the electrical modulation of the plasma frequency in TCOs, is rather highly localized at the discontinuities between the two materials, within few nanometers (the so-called *Debye length*), inside the accumulation/depletion area (Fig. 9b) [83,85–87]. This especially has been proved in systems modelled as parallel-plate capacitors based on TCOs in contact with HfO_2, Al_2O_3 or other dielectrics [70,73,74,82,83,88,89], but also in highly-doped ITO nanocrystals possessing cores and outer shells which are electrically-active [90,91]. For a variety of Metal-Oxide-Semiconductor (MOS) structures and TCO metasurfaces [23,74,85,89,92–94], low applied voltages (e.g. 5 V) blue-shift the specific optical features (e.g. reflectivity) because the refractive index is actively perturbed upon the formation of an accumulation region, at which plasmonic variables (ω_p, τ, etc.) vary accordingly.

Given these considerations, in the TCO-based PCs discussed in this work, electro-doping mechanisms may occur at the boundary between compact and porous layers, intrinsically characterized by higher defectivity [95]. However, this interpretation cannot justify completely the spectral shifts obtained. The reason can be found in the different optoelectronic properties of the porous component, for example with respect to the spin-coated TiO_2 nanoparticles used in ITO-TiO_2 PCs [16]. In the porous Ta:TiO_2 layer instead, although being the same material of the compact part, oxygen vacancies are lost due to the synthesis in high O_2 environment and high defectivity of the hierarchical nanostructure [28,96]. Consequently, Ta dopants are not efficiently activated and the amorphous nature is expected to impede the passage of carriers, even if mediated by oxygen-related defects, conversely to ITO-TiO_2 PCs [16] in which TiO_2 nanoparticles are crystalline. As last notice, the blue-shift of PBG features cannot be ascribed only to an overall modulation of ω_p in compact TCO layers, as the refractive index modulation of the conducting unit has been detected to be weak when an insulating interface is absent, also proved by simulations reported in Fig. S10 [16,35,70,97].

After all, the formation of an accumulation layer may contribute, in addition to electro-doping through defects, in reducing the refractive index at interfaces and thus determining the electro-optic PBG blue-shift. Nonetheless, the real extent of n variation is difficult to estimate, but some considerations can be made, according to Figs. 7 and 8.

We would expect that electro-doping contribution is higher when the

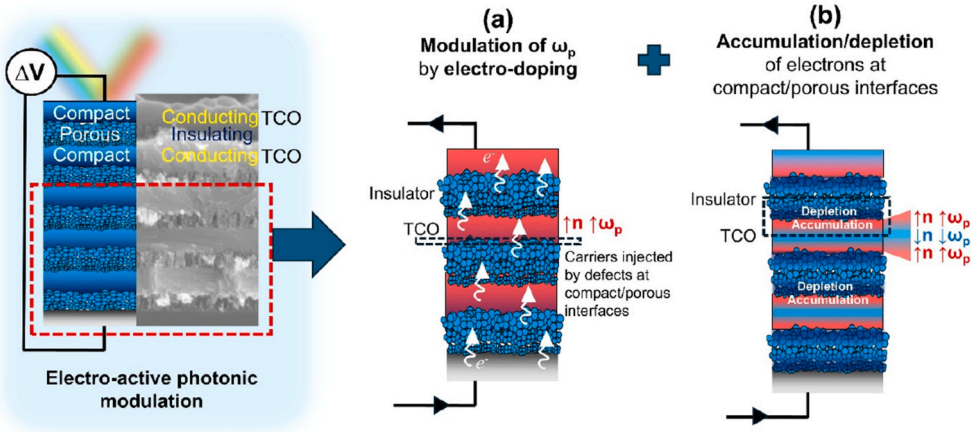

Fig. 9. Schematic representation of the main modulation mechanisms of carrier density occurring in electro-active TCO-based photonic crystals, under an applied potential. (a) Modulation of ω_p in the TCO layers promoted by electro-doping mediated through defects at interfaces, that rises the carrier density thus ω_p in the compact TCO layers. (b) Accumulation and depletion regions of electrons at TCO/insulator interfaces that modify locally the carrier density distribution.

porous layer is thinner, because carriers should travel shorter distances to reach the subsequent conducting layer before being trapped. On the contrary, the modulation mechanism given by carrier accumulation/depletion is not dependent from the thicknesses of the layers, as the Debye length extends only for few nm, much smaller than the characteristic thicknesses here involved (60–90 nm). Hence, the tunability of the PBG with TR, even if a clear trend cannot be identified (Fig. 8a and b), should be mainly ascribed to electro-doping processes, as shown in ITO-TiO_2 PCs [16].

As a final remark, redistribution of carriers in accumulation/depletion interfaces are not absent, due to the expected lower capability of carrier injection in the highly-defective porous layers, but perhaps play a secondary role. This hypothesis is supported by the enhanced PBG tunability fulfilled at larger Ta doping, attributed to the higher initial carrier density in TCO-based electro-optical modulators that is known to retrieve broader n variations within accumulation/depletion regions and consequently wider and intensified optical modulation [89,94].

Given this situation, the combination of electro-doping mechanisms and accumulation/depletion effects determines primarily the optical tunability, although further investigations should be performed to shed light on the contribution of these two concurring mechanism highlighted.

Anyhow, all Ta:TiO_2-based photonic crystals designed in this work advance previous investigations. Noticeable PBG shifts (16 nm with 5–7 V versus 25 nm with 10 V in ITO/TiO_2 PCs [16]) can be reached, due to the high homogeneity and optical quality (discussed in Fig. 6) enabled by the original synthesis approach. In particular, the PC geometry with similar compact/porous thicknesses (lowest TR) turns out to be the best compromise between quality of the optical PBG and electro-optic tunability. The essential point is that the PCs under discussion achieve similar tuning performance than those based on ITO and TiO_2 nanoparticles. It should be stressed that, unlike the well-known and commercially available ITO, which possesses one of the lowest resistivity (around $2 \times 10^{-4}\ \Omega$ cm) and highest mobility ($>30\ cm^2\ V^{-1}\ s^{-1}$) [20,68], Ta-doped TiO_2 TCO here employed shows more modest electrical properties (refer to Section 3.1). Nonetheless, the optical shifts of our PBGs are comparable, highlighting the significant potential of this alternative and earth-abundant TCO for actively-tunable photonics. This comparison underscores the efficacy of our approach, both in the fabrication and in the design of the device, even with less electrically-performant materials.

One of the most important benefits of solid-state active-tunable PCs is the capability to modulate the PBG properties under applied bias without the aid of liquid electrolytes.

If we define the figure of merit as the ratio between the wavelength change at the PBG shoulder over the voltage difference applied, it results much higher in liquid-based electro-tunable PCs. This because the shifts in PBG wavelength detected are typically in the order of tens and several tens of nm with very low voltages applied, e.g. few V, with color changing visible at naked eye [65,67].

In our case, we reach 16 nm of PBG tuning by applying 7 V, so the figure of merit previously defined is smaller than liquid-based devices. This seems to be a huge limitation in applicability, but it should be recalled that several materials typically employed in literature are intrinsically electrochromic, e.g. the well-known WO_3 [17].

In Table 2 we compared the type of systems, spectral shifts, applied voltages, use of electrolytes, and FoM. Electrolyte-based devices (conductive polymers, liquid crystals, or TCO nanocrystals) generally achieve larger shifts and higher FoM, typically at least twice those of all-solid-state systems (Moscardi et al. [16], Aluicio-Sarduy et al. [35], and this work. Nevertheless, the FoM of solid-state systems remains comparable, around 2–3.

Our approach is distinctive since it employs only Ta:TiO_2, in compact and porous layers with different doping levels, deposited in a single PLD step. Despite its lower electrical performance compared to ITO, Ta:TiO_2 enables comparable optical modulation thanks to the strong refractive index contrast arising from both morphology and charge-density/dielectric–metallic changes. This underlines the proof-of-concept value and the versatility of our method, which can be extended to other TCO-based systems. Although the performances between liquid-based and solid-state active tunable PCs are not comparable, we believe that the quite different entity of the optical modulation changes the targeted application. The PCs studied in this work results more appealing for biosensing of small refractive index changes, assisted by electrical stimuli, in the proximity of the PC, and/or for cheap anticounterfeit devices.

5. Conclusion

Active-tunable, one-dimensional photonic crystals multilayers all-based on Ta-doped TiO_2 TCO have been realized with a one-step and original approach based on an optimized process by pulsed laser deposition. Indeed, PLD is capable of mastering morphology, structure and overall optoelectronic properties of Ta:TiO_2 directly at the synthesis stage, by controlling solely the background deposition pressure of oxygen. Photonic crystals of Ta:TiO_2 with fixed Ta doping can be realized straightforward by alternating compact, crystalline and conducting Ta:TiO_2 layers obtained at low oxygen pressure (1 Pa) with nanoporous, amorphous and insulating blocks when the oxygen pressure rises (6 Pa). The resulting PCs possess high optical quality, as expected from the exceptional refractive index contrast (0.65) among inner constituents, with a PGB at 500–700 nm modulated according to the starting Ta doping level (5 % or 10 % at.) and the geometrical parameters (referred as thickness ratio between the compact and porous unit). This permitted to obtain an actively-tunable solid-state PC device in which the PBG spectral modulation is maximized by exploiting the inherent carrier density tunability of compact TCO layers, under the application of an external electrical stimulus. By switching on the electrical bias, electro-optical modulation has been tested on multilayers with different degree

Table 2
Comparative table of performances among different types of active tunable PCs.

Reference	Materials/System & Synthesis	Electrolyte	Max PBG shift	Max Bias Voltage	FoM (nm/V)
Heo et al., 2019 [17]	1D multilayer PCs with alternating doped nanocrystals (ITO, WO_{3-x}), fabricated via solution processing and layer-by-layer deposition	Liquid: 1 M LiTFSI in tetraglyme	~50–60 nm	~10 V	5–6
Li et al., 2024 [65] **(review)**	(1) Conducting polymers (PEDOT, PANI), deposited via spin coating or electrochemical polymerization (2) Infiltrated liquid crystals (LC PCs), fabricated via templating or capillary filling	(1) Solid/gel (2) Sealed LC cells	(1) 20–40 nm (2) up to 80 nm	(1) 10 V (2) 20 V	(1) 2–4 (2) 4
Jia et al., 2024 [67] **(review)**	(1) Electrochromic polymers, spin-coated or electrochemically deposited (2) LC photonic crystals	Various (gel or cell-based)	(1) 10–50 nm (2) up to 100 nm	(1) 10 V (2) 20 V	(1) 1–5 (2) 5
Moscardi et al., 2020 [16]	1D multilayer PCs with alternating nanoparticles ITO and TiO_2, fabricated via solution processing and layer-by-layer deposition	None (all-solid-state)	23 nm	10 V	2.3
Aluicio Sarduy et al., 2015 [35]	1D multilayer Ag/TiO_2 PCs for biosensing, prepared via deposition of multilayer on Ag substrate	None (all-solid-state)	10–15 nm	5 V	2–3
This work (Ta:TiO_2 PCs)	1D multilayer PCs of compact and porous Ta:TiO_2, fabricated via one-step PLD alternating dense and porous layers	None (all-solid-state)	16 nm	7 V	2.3

of doping (5 %, 10 % of Ta) and layer thicknesses. PBG position and width can be actively controlled (PBG shoulder shift of 11–16 nm) through the application of low external voltages (up to 7 V). The thickness ratio between compact and porous units plays a role in controlling the PBG shift, and the greatest modulation can be achieved when the thickness ratio is the lowest (thicker compact/conductive layers with thinner porous/insulating). Moreover, the higher is the degree of Ta doping, the higher is the degree of optical tunability. Nonetheless, the non-trivial mechanism behind still has to be fully understood, although it is associated to the overlap of different concomitant causes, such as primarily electro-doping and injection of carriers through defects at compact/porous boundaries (modification of the TCO plasma frequency, hence refractive index contrast), along with the formation of accumulation/depletion regions at inner interfaces, considering the PCs as capacitive systems, resulting in a very localized (within few nm) decrease/increase of the refractive index. This synthesis approach is particularly appealing and versatile since, in principle, it does not impose limits in thicknesses or number of layers in the PC and can be applied to various types of optical materials. Moreover, while this work investigated PBG in the visible spectrum, the method is adaptable for operation in the infrared range by adjusting layer thicknesses. Indeed, using Ta:TiO_2 is advantageous due to its lower plasma frequency with respect to most conventional TCOs, such as ITO, enabling carrier density modulation to shift further into the mid-IR region without suffering from plasmonic absorption in the near-IR, for devices engineering thermal regulation or precise molecule biosensing. This highlights the potential of our approach for creating tunable solid-state PCs across a wide wavelength range. While further optimization procedures in material properties, and in-depth analysis of the optical response are the next steps to accomplish, the PCs fabricated represent a promising avenue with potential for future developments, responding to the increasing demand for next-generation electro-active photonic devices where the PBG shifts fulfilled in this work enable precise optical modulation particularly suitable for anticounterfeit technologies and biosensing.

CRediT authorship contribution statement

Cristina Mancarella: Writing – review & editing, Writing – original draft, Visualization, Validation, Supervision, Methodology, Investigation, Funding acquisition, Formal analysis, Data curation, Conceptualization. **Liliana Moscardi:** Writing – review & editing, Visualization, Validation, Investigation, Formal analysis, Conceptualization. **Giancarlo Terraneo:** Writing – review & editing, Visualization, Validation, Investigation, Formal analysis, Conceptualization. **Alessio Lamperti:** Writing – review & editing, Visualization, Validation, Investigation, Conceptualization. **Marzia Iarossi:** Writing – review & editing, Visualization, Validation, Investigation, Formal analysis, Data curation, Conceptualization. **Francesco De Angelis:** Writing – review & editing, Visualization, Validation, Investigation, Conceptualization. **Francesco Scotognella:** Writing – review & editing, Visualization, Validation, Supervision, Investigation, Funding acquisition, Conceptualization. **Andrea Li Bassi:** Writing – review & editing, Visualization, Validation, Supervision, Funding acquisition, Conceptualization.

Notes

The authors declare no competing financial interest.

Declaration of competing interest

The authors declare the following financial interests/personal relationships which may be considered as potential competing interests: Andrea Li Bassi reports financial support was provided by Ministry of Education and Merit. Francesco Scotognella reports financial support was provided by Ministry of Education and Merit. If there are other authors, they declare that they have no known competing financial interests or personal relationships that could have appeared to influence the work reported in this paper.

Acknowledgements

C.M. and A.L.B. acknowledges funding by the National Recovery and Resilience Plan (NRRP), Mission 4, Component 2, Investment 1.3 - Call for tender No. 1561 of October 11, 2022 of Ministero dell'Università e della Ricerca (MUR) and by the European Union – NextGenerationEU, project code PE0000021, concession decree number 1561 of October 11, 2022 adopted by Ministero dell'Università e della Ricerca (MUR), CUP D43C22003090001, with project title "Network 4 Energy Sustainable Transition – NEST".

F. S. acknowledges funding by Ministero dell'Università e della Ricerca (MUR) (project ERACLITO 2022ZMA4X3).

Appendix A. Supplementary data

Supplementary data to this article can be found online at https://doi.org/10.1016/j.optmat.2025.117646.

Data availability

Data will be made available on request.

References

[1] Photonic Crystals, in: J.D. Joannopoulos (Ed.), Molding the Flow of Light, second ed., Princeton University Press, Princeton, 2008.
[2] H. Altug, D. Englund, J. Vučković, Ultrafast photonic crystal nanocavity laser, Nature Phys 2 (7) (2006) 484–488, https://doi.org/10.1038/nphys343.
[3] A. Chiappini, L.T.N. Tran, P.M. Trejo-García, L. Zur, A. Lukowiak, M. Ferrari, G. C. Righini, Photonic crystal stimuli-responsive chromatic sensors: a short review, Micromachines 11 (3) (2020) 290, https://doi.org/10.3390/mi11030290.
[4] A. Lonergan, C. Hu, C. O'Dwyer, Filling in the gaps: the nature of light transmission through solvent-filled inverse opal photonic crystals, Phys. Rev. Mater. 4 (6) (2020) 065201, https://doi.org/10.1103/PhysRevMaterials.4.065201.
[5] S. Liu, Y. Yang, L. Zhang, J. Xu, J. Zhu, Recent progress in responsive photonic crystals of block copolymers, J. Mater. Chem. C 8 (47) (2020) 16633–16647, https://doi.org/10.1039/D0TC04561F.
[6] S. John, Strong localization of photons in certain disordered Dielectric superlattices, Phys. Rev. Lett. 58 (23) (1987) 2486–2489, https://doi.org/10.1103/PhysRevLett.58.2486.
[7] K. Sakoda, Optical Properties of Photonic Crystals, second ed., Springer-Verlag, Berlin Heidelberg, 2005 https://doi.org/10.1007/b138376. Springer Series in Optical Sciences.
[8] A. Chiasera, F. Scotognella, L. Criante, S. Varas, G.D. Valle, R. Ramponi, M. Ferrari, Disorder in photonic structures induced by random layer thickness, Sci. Adv. Mater. 7 (6) (2015) 1207–1212, https://doi.org/10.1166/sam.2015.2249.
[9] F. Scotognella, A. Monguzzi, F. Meinardi, R. Tubino, DFB Laser action in a flexible fully plastic multilayer, Phys. Chem. Chem. Phys. 12 (2) (2009) 337–340, https://doi.org/10.1039/B917630F.
[10] L. Passoni, L. Criante, F. Fumagalli, F. Scotognella, G. Lanzani, F. Di Fonzo, Self-Assembled hierarchical nanostructures for high-efficiency porous photonic crystals, ACS Nano 8 (12) (2014) 12167–12174, https://doi.org/10.1021/nn5037202.
[11] M. Xu, J. Yu, Y. Song, R. Ran, W. Wang, Z. Shao, Advances in ceramic thin films fabricated by pulsed laser deposition for intermediate-temperature solid oxide fuel cells, Energy Fuels 34 (9) (2020) 10568–10582, https://doi.org/10.1021/acs.energyfuels.0c02338.
[12] A. Ojeda-G-P, M. Döbeli, T. Lippert, Influence of plume properties on thin film composition in pulsed laser deposition, Adv. Mater. Interfac. 5 (18) (2018) 1701062, https://doi.org/10.1002/admi.201701062.
[13] L. Moscardi, G. Lanzani, G.M. Paternò, F. Scotognella, Stimuli-Responsive photonic crystals, Appl. Sci. 11 (5) (2021) 2119, https://doi.org/10.3390/app11052119.
[14] M. Däntl, A. Jiménez-Solano, B.V. Lotsch, Stimuli-Responsive one-dimensional photonic crystals: design, fabrication and sensing, Mater. Adv. 3 (20) (2022) 7406–7424, https://doi.org/10.1039/D2MA00793B.
[15] L. Nucara, F. Greco, V. Mattoli, Electrically responsive photonic crystals: a review, J. Mater. Chem. C 3 (33) (2015) 8449–8467, https://doi.org/10.1039/C5TC00773A.
[16] L. Moscardi, G.M. Paternò, A. Chiasera, R. Sorrentino, F. Marangi, I. Kriegel, G. Lanzani, F. Scotognella, Electro-Responsivity in electrolyte-free and solution processed Bragg Stacks, J. Mater. Chem. C (2020), https://doi.org/10.1039/D0TC02437F.

[17] S. Heo, A. Agrawal, D.J. Milliron, Wide dynamic range in tunable electrochromic bragg stacks from doped semiconductor nanocrystals, Adv. Funct. Mater. 29 (37) (2019) 1904555, https://doi.org/10.1002/adfm.201904555.

[18] E. Redel, J. Mlynarski, J. Moir, F.M. Ali, C. Huai, S. Petrov, M.G. Helander, F. C. Peiris, G. Von Freymann, G.A. Ozin, Electrochromic Bragg Mirror: ECBM, Adv. Mater. 24 (35) (2012), https://doi.org/10.1002/adma.201202484.

[19] L. Xiao, Y. Lv, J. Lin, Y. Hu, W. Dong, X. Guo, Y. Fan, N. Zhang, J. Zhao, Y. Wang, X. Liu, WO $_3$ -Based electrochromic distributed bragg reflector: toward electrically tunable microcavity luminescent device, Adv. Opt. Mater. 6 (1) (2018) 1700791, https://doi.org/10.1002/adom.201700791.

[20] Z. Wang, C. Chen, K. Wu, H. Chong, H. Ye, Transparent conductive oxides and their applications in near infrared plasmonics, Phys. Status Solidi 216 (5) (2019) 1700794, https://doi.org/10.1002/pssa.201700794.

[21] V.E. Babicheva, A. Boltasseva, A.V. Lavrinenko, Transparent conducting oxides for electro-optical plasmonic modulators, Nanophotonics 4 (1) (2015) 165–185, https://doi.org/10.1515/nanoph-2015-0004.

[22] W. Jaffray, S. Saha, V.M. Shalaev, A. Boltasseva, M. Ferrera, Transparent conducting oxides: from all-dielectric plasmonics to a new paradigm in integrated photonics, Adv. Opt Photon 14 (2) (2022) 148, https://doi.org/10.1364/AOP.448391.

[23] Y.-W. Huang, H.W.H. Lee, R. Sokhoyan, R.A. Pala, K. Thyagarajan, S. Han, D. P. Tsai, H.A. Atwater, Gate-Tunable conducting oxide metasurfaces, Nano Lett. 16 (9) (2016) 5319–5325, https://doi.org/10.1021/acs.nanolett.6b00555.

[24] G.M. Paternò, L. Moscardi, I. Kriegel, F. Scotognella, G. Lanzani, Electro-Optic and magneto-optic photonic devices based on Multilayer photonic structures, J. Photon. Energy 8 (3) (2018) 1, https://doi.org/10.1117/1.JPE.8.032201.

[25] I. Kriegel, F. Scotognella, L. Manna, Plasmonic doped semiconductor nanocrystals: properties, fabrication, applications and perspectives, Phys. Rep. 674 (2017) 1–52, https://doi.org/10.1016/j.physrep.2017.01.003.

[26] A. Agrawal, R.W. Johns, D.J. Milliron, Control of localized surface plasmon resonances in metal oxide nanocrystals, Annu. Rev. Mater. Res. 47 (1) (2017) 1–31, https://doi.org/10.1146/annurev-matsci-070616-124259.

[27] O. Zandi, A. Agrawal, A.B. Shearer, L.C. Reimnitz, C.J. Dahlman, C.M. Staller, D. J. Milliron, Impacts of surface depletion on the plasmonic properties of doped semiconductor nanocrystals, Nat. Mater. 17 (8) (2018) 710–717, https://doi.org/10.1038/s41563-018-0130-5.

[28] P. Mazzolini, P. Gondoni, V. Russo, D. Chrastina, C.S. Casari, A. Li Bassi, Tuning of electrical and optical properties of highly conducting and transparent Ta-Doped TiO $_2$ polycrystalline films, J. Phys. Chem. C 119 (13) (2015) 6988–6997, https://doi.org/10.1021/jp5126156.

[29] P. Mazzolini, V. Russo, C.S. Casari, T. Hitosugi, S. Nakao, T. Hasegawa, A. Li Bassi, Vibrational–Electrical properties relationship in donor-doped TiO $_2$ by Raman spectroscopy, J. Phys. Chem. C 120 (33) (2016) 18878–18886, https://doi.org/10.1021/acs.jpcc.6b05282.

[30] P. Mazzolini, T. Acartürk, D. Chrastina, U. Starke, C.S. Casari, G. Gregori, A. L. Bassi, Controlling the electrical properties of Undoped and Ta-Doped TiO $_2$ polycrystalline films via ultra-fast-annealing treatments, Adv. Electron. Mater. 2 (3) (2016) 1500316, https://doi.org/10.1002/aelm.201500316.

[31] B.R.R. Bricchi, M. Sygletou, L. Ornago, G. Terraneo, F. Bisio, C. Mancarella, L. Stasi, F. Rusconi, E. Mogni, M. Ghidelli, P. Biagioni, A.L. Bassi, Optical and electronic properties of transparent conducting Ta:TiO2 thin and ultra-thin films: effect of doping and thickness, Mater. Adv. (2021), https://doi.org/10.1039/D1MA00584G.

[32] P. Deák, B. Aradi, T. Frauenheim, Oxygen deficiency in Ti O 2 : similarities and differences between the Ti self-interstitial and the O vacancy in bulk rutile and anatase, Phys. Rev. B 92 (4) (2015) 045204, https://doi.org/10.1103/PhysRevB.92.045204.

[33] I. Kriegel, F. Scotognella, Modelling and fabrication of one-dimensional flexible Multilayer photonic crystals based on polymers and inorganic materials, Opt. Mater. 123 (2022) 111859, https://doi.org/10.1016/j.optmat.2021.111859.

[34] M. Born, E. Wolf, Principles of Optics: Electromagnetic Theory of Propagation, Interference and Diffraction of Light, Cambridge University Press, 2000.

[35] E. Aluicio-Sarduy, S. Callegari, D.G. Figueroa del Valle, A. Desii, I. Kriegel, F. Scotognella, Electric field induced structural colour tuning of a Silver/Titanium dioxide nanoparticle one-dimensional photonic crystal, Beilstein J. Nanotechnol. 7 (2016) 1404–1410, https://doi.org/10.3762/bjnano.7.131.

[36] B.R. Bricchi, M. Ghidelli, L. Mascaretti, A. Zapelli, V. Russo, C.S. Casari, G. Terraneo, I. Alessandri, C. Ducati, A. Li Bassi, Integration of Plasmonic Au Nanoparticles in TiO2 Hierarchical Structures in a Single-Step Pulsed Laser Co-Deposition, Mater. Des. 156 (2018) 311–319, https://doi.org/10.1016/j.matdes.2018.06.051.

[37] Y. Hara, T. Garvey, L. Alibabaei, R. Ghosh, R. Lopez, Controlled seeding of laser deposited ta:tio $_2$ nanobrushes and their performance as photoanode for Dye sensitized solar cells, ACS Appl. Mater. Interfaces 5 (24) (2013) 13140–13145, https://doi.org/10.1021/am404176q.

[38] Database Minkrist, TiO2 Anatase, Card 190. https://database.iem.ac.ru/mincryst/s_carta.php?ANATASE+190.

[39] Database Minkrist, TiO2 Rutile, Card 4028. https://database.iem.ac.ru/s_carta.php?4028.

[40] T.M.R. Viseu, B. Almeida, M. Stchakovsky, B. Drevillon, M.I.C. Ferreira, J.B. Sousa, Optical characterisation of anatase: a comparative Study of the bulk crystal and the polycrystalline thin film, Thin Solid Films 401 (1–2) (2001) 216–224, https://doi.org/10.1016/S0040-6090(01)01479-1.

[41] R. Gago, S. Prucnal, D. Esteban-Mendoza, Soft X-Ray absorption Study of tantalum incorporation in titanium oxide films: impact of flash-lamp annealing, Ceram. Int. 46 (10) (2020) 15772–15778, https://doi.org/10.1016/j.ceramint.2020.03.121.

[42] M. Tsutsumi, H. Tanaka, Understanding the change in electrical resistance of TiO $_2$ thin film irradiated with YVO $_4$ third-harmonic generation pulse laser, Int. J. Appl. Ceram. Technol. (2022) 14193, https://doi.org/10.1111/ijac.14193 ijac.

[43] D.K. Pallotti, L. Passoni, F. Gesuele, P. Maddalena, F. Di Fonzo, S. Lettieri, Giant O $_2$ -Induced photoluminescence modulation in hierarchical titanium dioxide nanostructures, ACS Sens. 2 (1) (2017) 61–68, https://doi.org/10.1021/acssensors.6b00432.

[44] F. Di Fonzo, C.S. Casari, V. Russo, M.F. Brunella, A. Li Bassi, C.E. Bottani, Hierarchically organized nanostructured TiO $_2$ for photocatalysis applications, Nanotechnology 20 (1) (2009) 015604, https://doi.org/10.1088/0957-4484/20/1/015604.

[45] S.A. Kim, Sk K. Hussain, M.A. Abbas, J.H. Bang, High-Temperature solid-state rutile-to-anatase phase transformation in TiO2, J. Solid State Chem. 315 (2022) 123510, https://doi.org/10.1016/j.jssc.2022.123510.

[46] H. Rotella, B. Caby, Y. Ménesguen, Y. Mazel, A. Valla, D. Ingerle, B. Detlefs, M.-C. Lépy, A. Novikova, G. Rodriguez, C. Streli, E. Nolot, Elemental depth profiling in transparent conducting oxide thin film by X-Ray reflectivity and grazing incidence X-Ray fluorescence combined analysis, Spectrochim. Acta B Atom Spectrosc. 135 (2017) 22–28, https://doi.org/10.1016/j.sab.2017.06.011.

[47] Webmineral.Com. https://doi.org/webmineral.com.

[48] Mindat.Org. https://doi.org/mindat.org.

[49] B. Cui, L. Zeng, D. Keane, M.J. Bedzyk, D.B. Buchholz, R.P.H. Chang, X. Yu, J. Smith, T.J. Marks, Y. Xia, A.F. Facchetti, J.E. Medvedeva, M. Grayson, Thermal conductivity comparison of Indium Gallium Zinc oxide thin films: dependence on temperature, crystallinity, and porosity, J. Phys. Chem. C 120 (14) (2016) 7467–7475, https://doi.org/10.1021/acs.jpcc.5b12105.

[50] L. Mascaretti, V. Russo, G. Zoppellaro, A. Lucotti, C.S. Casari, Š. Kment, A. Naldoni, A. Li Bassi, Excitation Wavelength- and medium-dependent photoluminescence of reduced nanostructured TiO $_2$ films, J. Phys. Chem. C 123 (17) (2019) 11292–11303, https://doi.org/10.1021/acs.jpcc.9b01727.

[51] R.V. Nair, V.S. Gummaluri, M.V. Matham, V. C, A review on optical bandgap engineering in TiO $_2$ nanostructures via doping and intrinsic vacancy modulation towards visible light applications, J. Phys. D Appl. Phys. 55 (31) (2022) 313003, https://doi.org/10.1088/1361-6463/ac6135.

[52] L. Shi, Z. Li, T.D. Dao, T. Nagao, Y. Yang, A Synergistic Interaction between Isolated Au Nanoparticles and Oxygen Vacancies in an Amorphous Black TiO $_2$ Nanoporous Film: toward Enhanced Photoelectrochemical Water Splitting, J. Mater. Chem. A 6 (27) (2018) 12978–12984, https://doi.org/10.1039/C8TA04621B.

[53] O. Berger, Understanding the fundamentals of TiO $_2$ surfaces. Part I. The influence of defect States on the correlation between crystallographic structure, electronic structure and physical properties of single-crystal surfaces, Surf. Eng. 38 (2) (2022) 91–149, https://doi.org/10.1080/02670844.2022.2063482.

[54] S. Normani, P. Bertolotti, F. Bisio, M. Magnozzi, F. Federico, S. Filattiera, S. Perotto, F. Marangi, G. Lanzani, G.M. Paternò, Tamm plasmon resonance as optical fingerprint of Silver/Bacteria interaction, Tamm Plasmon Resonance as Optical Fingerprint of Silver/Bacteria Interaction 15 (23) (2023) 27750–27758, https://doi.org/10.1021/acsami.3c05473.

[55] R. Georgiev, K. Lazarova, M. Vasileva, T. Babeva, All Niobia bragg stacks for optical sensing of vapors, Opt. Quant. Electron. 52 (2) (2020) 114, https://doi.org/10.1007/s11082-020-2243-8.

[56] P.G. O'Brien, D.P. Puzzo, A. Chutinan, L.D. Bonifacio, G.A. Ozin, N.P. Kherani, Selectively transparent and conducting photonic crystals, Adv. Mater. 22 (5) (2010) 611–616, https://doi.org/10.1002/adma.200902605.

[57] L.D. Bonifacio, B.V. Lotsch, D.P. Puzzo, F. Scotognella, G.A. Ozin, Stacking the nanochemistry deck: structural and compositional diversity in one-dimensional photonic crystals, Adv. Mater. 21 (16) (2009) 1641–1646, https://doi.org/10.1002/adma.200802348.

[58] D.Y. Lee, J.-H. Park, Y.-H. Kim, M.-H. Lee, N.-I. Cho, Effect of Nb doping on morphology, crystal structure, optical band gap energy of TiO2 thin films, Curr. Appl. Phys. 14 (3) (2014) 421–427, https://doi.org/10.1016/j.cap.2013.12.025.

[59] C. Bohórquez, H. Bakkali, J.J. Delgado, E. Blanco, M. Herrera, M. Domínguez, Spectroscopic ellipsometry Study on tuning the electrical and optical properties of Zr-Doped ZnO thin films grown by atomic layer deposition, ACS Appl. Electron. Mater. 4 (3) (2022) 925–935, https://doi.org/10.1021/acsaelm.1c01026.

[60] J.A. Hillier, S. Camelio, W. Cranton, A.V. Nabok, C.J. Mellor, D.C. Koutsogeorgis, N. Kalfagiannis, When ellipsometry works best: a case Study with transparent conductive oxides, ACS Photonics 7 (10) (2020) 2692–2702, https://doi.org/10.1021/acsphotonics.0c00389.

[61] Y. Wu, K. Zhang, B. Yang, Ordered Hybrid Micro/Nanostructures and their optical applications, Adv. Opt. Mater. 7 (7) (2019) 1800980, https://doi.org/10.1002/adom.201800980.

[62] J. Kim, L.J. Krayer, J.L. Garrett, J.N. Munday, Interfacial defect-mediated near-infrared silicon photodetection with metal oxides, ACS Appl. Mater. Interfaces 11 (50) (2019) 47516–47524, https://doi.org/10.1021/acsami.9b14953.

[63] J. Low, L. Zhang, B. Zhu, Z. Liu, J. Yu, TiO $_2$ photonic crystals with localized surface photothermal effect and enhanced photocatalytic CO $_2$ reduction activity, ACS Sustainable Chem. Eng. 6 (11) (2018) 15653–15661, https://doi.org/10.1021/acssuschemeng.8b04150.

[64] J. Ge, Y. Yin, Responsive photonic crystals, Angew. Chem. Int. Ed. 50 (7) (2011) 1492–1522, https://doi.org/10.1002/anie.200907091.

[65] L. Li, Z. Yu, C. Ye, Y. Song, Structural color boosted electrochromic devices: strategies and applications, Adv. Funct. Mater. 34 (12) (2024) 2311845, https://doi.org/10.1002/adfm.202311845.

[66] M. Li, D. Liu, H. Cheng, L. Peng, M. Zu, Manipulating metals for adaptive thermal camouflage, Sci. Adv. 6 (22) (2020) eaba3494, https://doi.org/10.1126/sciadv.aba3494.
[67] R. Jia, S. Xiang, Y. Wang, H. Chen, M. Xiao, Electrically triggered color-changing materials: mechanisms, performances, and applications, Adv. Opt. Mater. 12 (10) (2024) 2302222, https://doi.org/10.1002/adom.202302222.
[68] Z. Ma, Z. Li, K. Liu, C. Ye, V.J. Sorger, Indium-Tin-Oxide for high-performance electro-optic modulation, Nanophotonics 4 (1) (2015) 198–213, https://doi.org/10.1515/nanoph-2015-0006.
[69] I.C. Reines, M.G. Wood, T.S. Luk, D.K. Serkland, S. Campione, Compact epsilon-near-zero silicon photonic phase modulators, Opt. Express 26 (17) (2018) 21594, https://doi.org/10.1364/OE.26.021594.
[70] E. Feigenbaum, K. Diest, H.A. Atwater, Unity-Order Index change in transparent conducting oxides at visible frequencies, Nano Lett. 10 (6) (2010) 2111–2116, https://doi.org/10.1021/nl1006307.
[71] X. Liu, J.-H. Kang, H. Yuan, J. Park, Y. Cui, H.Y. Hwang, M.L. Brongersma, Tuning of plasmons in transparent conductive oxides by carrier accumulation, ACS Photonics 5 (4) (2018) 1493–1498, https://doi.org/10.1021/acsphotonics.7b01517.
[72] S.A. Maier, Plasmonics: Fundamentals and Applications, Springer US, New York, NY, 2007, https://doi.org/10.1007/0-387-37825-1.
[73] X. Li, Q. Cheng, S. Guo, Z. Li, Research of gate-tunable phase modulation metasurfaces based on epsilon-near-zero property of indium-tin-oxide, Photonics 9 (5) (2022) 323, https://doi.org/10.3390/photonics9050323.
[74] Z. Lu, K. Shi, P. Yin, Nanoscale field effect optical modulators based on depletion of epsilon-near-zero films, Opt. Commun. 381 (2016) 18–23, https://doi.org/10.1016/j.optcom.2016.06.057.
[75] F. Novelli, D. Fausti, F. Giusti, F. Parmigiani, M. Hoffmann, Mixed regime of light-matter interaction revealed by phase sensitive measurements of the dynamical franz-keldysh effect, Sci. Rep. 3 (1) (2013) 1227, https://doi.org/10.1038/srep01227.
[76] A.K. Pradhan, R.M. Mundle, K. Santiago, J.R. Skuza, B. Xiao, K.D. Song, M. Bahoura, R. Cheaito, P.E. Hopkins, Extreme tunability in aluminum doped zinc oxide plasmonic materials for near-infrared applications, Sci. Rep. 4 (1) (2014) 6415, https://doi.org/10.1038/srep06415.
[77] C.J. Dahlman, A. Agrawal, C.M. Staller, J. Adair, D.J. Milliron, Anisotropic origins of localized surface plasmon resonance in N-Type anatase TiO_2 nanocrystals, Chem. Mater. 31 (2) (2019) 502–511, https://doi.org/10.1021/acs.chemmater.8b04519.
[78] A. Barman, D. Das, S. Deshmukh, P.K. Sarkar, D. Banerjee, R. Hübner, M. Gupta, C. P. Saini, S. Kumar, P. Johari, S. Dhar, A. Kanjilal, Aliovalent ta-doping-engineered oxygen vacancy configurations for ultralow-voltage resistive memory devices: a DFT-Supported experimental Study, ACS Appl. Mater. Interfaces 14 (30) (2022) 34822–34834, https://doi.org/10.1021/acsami.2c05089.
[79] E. Battal, A. Ozcan, A.K. Okyay, Resistive switching-based electro-optical modulation, Adv. Opt. Mater. 2 (12) (2014) 1149–1154, https://doi.org/10.1002/adom.201400209.
[80] G. Di Martino, S. Tappertzhofen, S. Hofmann, J. Baumberg, Nanoscale plasmon-enhanced spectroscopy in memristive switches, Small 12 (10) (2016) 1334–1341, https://doi.org/10.1002/smll.201503165.
[81] S. Boyeras Baldomá, S.M. Pazos, F.L. Aguirre, G. Ankonina, L. Kornblum, E. Yalon, F. Palumbo, Wear-out and breakdown of Ta2O5/Nb:SrTiO3 stacks, Solid State Electron. 198 (2022) 108462, https://doi.org/10.1016/j.sse.2022.108462.
[82] J. Park, J.-H. Kang, X. Liu, M.L. Brongersma, Electrically tunable epsilon-near-zero (ENZ) metafilm absorbers, Sci. Rep. 5 (1) (2015) 15754, https://doi.org/10.1038/srep15754.
[83] L. Li, H. Hao, H. Zhao, Time and voltage dependences of nanoscale dielectric constant modulation on indium Tin oxide films, Mater. Res. Express 4 (1) (2017) 016402, https://doi.org/10.1088/2053-1591/aa51e7.
[84] I.A. Pshenichnyuk, S.S. Kosolobov, V.P. Drachev, Fine-Tuning of the electro-optical switching behavior in indium tin oxide, Phys. Rev. B 103 (11) (2021) 115404, https://doi.org/10.1103/PhysRevB.103.115404.
[85] L. Wen, X. Nan, J. Li, D.R.S. Cumming, X. Hu, Q. Chen, Broad-Band spatial light modulation with dual epsilon-near-zero modes, OEA 5 (6) (2022), https://doi.org/10.29026/oea.2022.200093, 200093–200093.
[86] Y. Wang, H. Zhao, D. Huo, H. Su, C. Wang, J. Zhang, Accumulation-Layer hybridized surface plasmon polaritions at an ITO/$LiNbO_3$ interface, Opt. Lett. 44 (4) (2019) 947, https://doi.org/10.1364/OL.44.000947.
[87] S. Fardad, E. Alexander Ramos, A. Salandrino, Accumulation-Layer surface plasmons in transparent conductive oxides, Opt. Lett. 42 (10) (2017) 2038, https://doi.org/10.1364/OL.42.002038.
[88] D. Ghindani, A.R. Rashed, M. Habib, H. Caglayan, Gate tunable coupling of Epsilon-Near-Zero and plasmonic modes, Adv. Opt. Mater. 9 (22) (2021) 2100800, https://doi.org/10.1002/adom.202100800.
[89] M. Sygletou, S. Benedetti, A. di Bona, M. Canepa, F. Bisio, E. Bellingeri, In-Operando optical spectroscopy of field-effect-gated Al-Doped ZnO, ACS Appl. Mater. Interfaces (2023), https://doi.org/10.1021/acsami.2c16668 acsami.2c16668.
[90] P. Yin, Y. Tan, H. Fang, M. Hegde, P.V. Radovanovic, Plasmon-Induced carrier polarization in semiconductor nanocrystals, Nat. Nanotechnol. 13 (6) (2018) 463–467, https://doi.org/10.1038/s41565-018-0096-0.
[91] M. Ghini, N. Curreli, M.B. Lodi, N. Petrini, M. Wang, M. Prato, A. Fanti, L. Manna, I. Kriegel, Control of Electronic Band profiles through depletion layer engineering in Core–Shell nanocrystals, Nat. Commun. 13 (1) (2022) 537, https://doi.org/10.1038/s41467-022-28140-y.
[92] J. Zhang, J. Yang, M. Schell, A. Anopchenko, L. Tao, Z. Yu, H.W.H. Lee, Gate-Tunable optical filter based on conducting oxide metasurface heterostructure, Opt. Lett. 44 (15) (2019) 3653, https://doi.org/10.1364/OL.44.003653.
[93] A. Anopchenko, S. Gurung, L. Tao, C. Arndt, H.W.H. Lee, Atomic layer deposition of ultra-thin and smooth Al-Doped ZnO for zero-index photonics, Mater. Res. Express 5 (1) (2018) 014012, https://doi.org/10.1088/2053-1591/aaa653.
[94] A. Anopchenko, L. Tao, C. Arndt, H.W.H. Lee, Field-Effect tunable and broadband epsilon-near-zero perfect absorbers with deep subwavelength thickness, ACS Photonics 5 (7) (2018) 2631–2637, https://doi.org/10.1021/acsphotonics.7b01373.
[95] E. Bellingeri, S. Rusponi, A. Lehnert, H. Brune, F. Nolting, A. Leveratto, A. Plaza, D. Marré, Influence of free charge carrier density on the magnetic behavior of (Zn, Co)O thin film studied by field effect modulation of magnetotransport, Sci. Rep. 9 (1) (2019) 149, https://doi.org/10.1038/s41598-018-36336-w.
[96] A.R. Barman, M. Motapothula, A. Annadi, K. Gopinadhan, Y.L. Zhao, Z. Yong, I. Santoso, Ariando, M. Breese, A. Rusydi, S. Dhar, T. Venkatesan, Multifunctional Ti1−xTaxO2: ta doping or alloying? Appl. Phys. Lett. 98 (7) (2011) 072111 https://doi.org/10.1063/1.3553773.
[97] G.M. Paternò, C. Iseppon, A. D'Altri, C. Fasanotti, G. Merati, M. Randi, A. Desii, E. A.A. Pogna, D. Viola, G. Cerullo, F. Scotognella, I. Kriegel, Solution processable and optically switchable 1D photonic structures, Sci. Rep. 8 (1) (2018) 1–8, https://doi.org/10.1038/s41598-018-21824-w.